Int. J. Environ. Sci. Technol. (2014) 11:997–1006
DOI 10.1007/s13762-013-0465-z

ORIGINAL PAPER

# Removal of $H_2S$ from crude oil via stripping followed by adsorption using ZnO/MCM-41 and optimization of parameters

**N. Hazrati · M. Abdouss · A. Vahid ·**
**A. A. Miran Beigi · A. Mohammadalizadeh**

Received: 11 December 2012 / Revised: 15 November 2013 / Accepted: 7 December 2013 / Published online: 10 January 2014

**Abstract** In the present work, $H_2S$ of crude oil was removed via a two-step method including stripping followed by adsorption. First, ZnO/MCM-41 adsorbents containing 5, 17.5 and 30 wt% of zinc were synthesized and characterized using XRD and nitrogen physisorption. Then, these materials were used as adsorbents for the removal of the $H_2S$ stripped from crude oil. At second step, the $H_2S$ of crude oil was extracted to gas phase by hot stripping. The obtained extract was collected in a storage tank for the subsequent $H_2S$ adsorption process. A three-factor Box–Behnken design with five center points and one response was performed for the optimization of adsorption of $H_2S$. The influence of process parameters and their interactional effects on the adsorption of $H_2S$ were analyzed using the obtained adsorption experimental data. A model including three important factors, i.e., temperature, space velocity and amount of supported zinc and their interactions, was developed to generate the optimum condition. The point of $Zn = 30$ wt%, $T = 300$ °C and space velocity $= 3{,}000\ h^{-1}$ had the optimum point with the highest break point time ($t_{bp} = 973$ min).

**Keywords** Box–Behnken design · Crude oil · Hydrogen sulfide · Mesoporous materials · Optimization · Removal · Zinc oxide

## Introduction

Hydrogen sulfide, $H_2S(g)$, is a common gaseous pollutant which is colorless, odorous, highly toxic, corrosive for pipelines and poisonous for catalysts (Husein et al. 2010; Nassar et al. 2010; Wieckowska 1995; Rowan et al. 2009; Dorman et al. 2002). The world demand for sweet crude oil as well as lowering the emitted pollutants from crude oil derivatives is growing to meet international regulations. In the combustion of fuels containing sulfur such as coal and oil, $SO_x$ is mostly formed. $SO_x$ is responsible for the formation of acid rain, corrosion of metal structures and is harmful to human and other living organisms (Hogan 2010; Holleman and Wiberg 2001). Removal of $H_2S$ from a gas stream could be accomplished by adsorption onto a solid surface (Srivastav and Srivastava 2009; Samadi-Maybodi et al. 2011; Wang et al. 2012; Ko et al. 2004), catalytic oxidation and absorption using a liquid solution (Morais Batista et al. 2010; Corma et al. 1995). However, the majority of these techniques show some drawbacks. For instance, high surface area activated carbons are expensive, and the catalytic oxidation materials (Morais Batista et al. 2010) and liquid solution could cause secondary pollution after invalidation. Liquid-phase chemical scrubbing with amines suffers from inherently high regeneration cost and inefficiency (Corma et al. 1995). Many materials have been developed for $H_2S$ adsorption from a great amount of industrial gas effluent streams (Untea et al. 2009; Subrenat et al. 2008; Bagreev et al. 2004; Polychronopoulou et al. 2005). Adsorption by metal oxide sorbents is recognized to be an energy-efficient technology for $H_2S$ removal. Sorbents with high surface area and high porosity are needed to increase the sorption activity and to increase the break point time. In order for the high surface area to be accessible, a network of macropores and mesopores should be existed in

N. Hazrati · M. Abdouss
Department of Chemistry, Amirkabir University of Technology, Tehran, Iran

N. Hazrati · A. Vahid (✉) · A. A. Miran Beigi · A. Mohammadalizadeh
Research Institute of Petroleum Industry, Tehran, Iran
e-mail: avahid753@gmail.com

the sorbent. Mesoporous silicate materials are good candidates and can be used for this purpose. One of the well-known members of this group, i.e., MCM-41, has allowed immense scope for many research groups to work on this material, with uniform pore size and shape, in different ways due to its very high surface area and adsorption capacity (Kresge et al. 1992; Wan and Zhao 2007; Taguchi and Schuth 2005; Li et al. 2010; Galarneau et al. 1999). One of the appropriate methods for the preparation of such sorbent is embedding of proper metal oxides (active part) on the surface of MCM-41 (Samadi-Maybodi et al. 2011). Thermodynamic analysis of the oxides of some metals showed that Zn, Fe, Mo, Mn, Sr, B, Co, Cu and W are the suitable metals due to their sulfur removal efficiencies and thermal stabilities (Wang et al. 2009).

After the work of Westmoreland and Harrison, studies were concentrated on zinc, copper, iron and calcium oxides (Wang et al. 2009). From the thermodynamic analysis, it can be shown that zinc oxide is a good adsorbent having high sulfur removal efficiency because of high equilibrium constant (Westmoreland and Harrison 1976; Wang et al. 2008). Moreover, ZnO is considered a cost-effective and stable sorbent compared to other metal oxides (Westmoreland and Harrison 1976). Experimental design methods help us to find the influences of each process parameter and their interactions to achieve the optimum condition (Sun et al. 2007; Kumar et al. 2008; Tripathi et al. 2009; Habibi et al. 2010; Mohammadalizadeh et al. 2011a, b; Keyvanloo et al. 2010; Farahzadi et al. 2012). Herein, the $H_2S$ of crude oil was removed via stripping followed by adsorption on zinc-containing MCM-41. At first, different incipient wetness prepared zinc-containing MCM-41 adsorbents were synthesized and characterized using high- and low-angle X-ray diffraction and nitrogen physisorption. Then, the $H_2S$ of crude oil was removed via hot stripping. The obtained $H_2S$-in-LPG extract was collected in a storage tank. After that, the $H_2S$ of obtained $H_2S$-in-LPG extract was adsorbed using zinc-containing MCM-41. Response surface methodology (RSM) was applied for optimizing the adsorption of $H_2S$. A three-factor Box–Behnken design with five center points and one response was performed to generate the optimum condition. This work was carried out at research institute of petroleum industry during winter 2012.

## Materials and methods

### Synthesis

All chemicals were purchased from Merck and used without further purification. In a typical synthesis, cetyltrimethylammonium bromide (CTAB) and NaOH were dissolved in an appropriate amount of water. While stirring, predetermined quantity of tetraethylorthosilicate (TEOS) was added to this solution over a period of 15 min. After 70-min stirring, the obtained suspension was transferred into the Teflon-lined stainless steel and autoclaved at 90 °C for 96 h. Then, the precipitate was filtered and washed with deionized water and acetone, respectively. The as-synthesized samples were calcined with heating rate of 1 °C/min up to 550 °C and held at this temperature for 5 h.

For the preparation of zinc-containing MCM-41, 10 grams of calcined sample was impregnated with 100 mL of tetrahydrofuran (THF) containing predetermined amounts of $Zn(NO_3)_2 \cdot 4H_2O$. The suspension was shacked for 24 h and dried under vacuum at 80 °C and calcined at 550 °C for 3 h. Resultant samples denoted as ZnO*x*/MCM where *x* indicates the weight percent of zinc in the corresponding sample.

### Characterization

X-ray diffraction (XRD) patterns were recorded using a Philips 1840 diffractometer with nickel-filtered Cu Kα radiation (1.5418° A) operating at 35.4 kV and 28 mA. The BET surface area, pore volume and pore size distribution of synthesized samples were measured by nitrogen adsorption at 77 K using a BELSORP-max apparatus. Prior to analysis, the samples were out-gassed in vacuum for 4 h at 300 °C until a stable vacuum of 0.1 Pa was reached. Determination of $H_2S$ was carried out via UOP-163 standard test method using METTLER TOLEDO G20 apparatus.

### $H_2S$ adsorption

Soumar crude oil was obtained from south of Iran. At first, $H_2S$ of crude oil was removed using hot stripping and the obtained extract was collected in a storage tank. The obtained extract containing light hydrocarbons, such as LPG, lighter gases and also $H_2S$, was abbreviated to $H_2S$-in-LPG. The stripping was carried out at 80 °C during 30 min under the 0.5 L/min flow rate of nitrogen as carrier gas. The concentration of $H_2S$ in the stripped crude oil was lower than 1 ppm. The concentration of $H_2S$ in the $H_2S$-in-LPG was 5,000 ppm. This concentration was taken as the criterion for the $H_2S$ break point during adsorption of $H_2S$. Adsorption measurements for $H_2S$ were performed using a laboratory-made apparatus. Scheme 1 illustrates the adsorption apparatus made and used in this work.

Analysis of the reactor effluent stream using UOP163 method gave $H_2S$ break point curves.

### Box–Behnken experimental design and optimization by RSM

The optimum condition for maximizing the adsorption of $H_2S$ was determined by means of a three-factor Box–

**Scheme 1** Schematic representation of laboratory-made apparatus used for the removal of $H_2S$ from crude oil

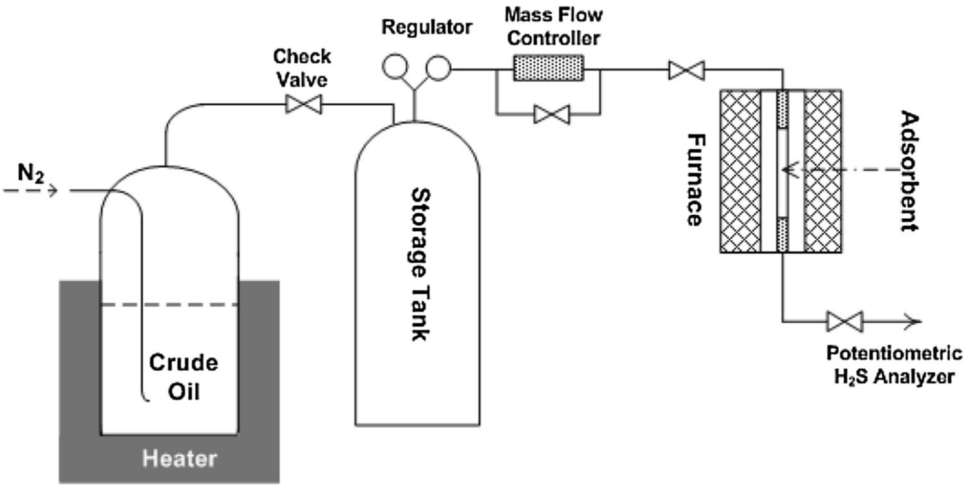

Behnken design combined with response surface modeling and quadratic model. The effect of quadratic interactions and main effects on adsorption of $H_2S$ were investigated as well. It is well known that this experimental method gave $H_2S$ breakthrough curves to model the response as a mathematical function of factors with unbiased and minimum variance. Thus, the graphical outlook of the mathematical model describes the shape of the response surface being investigated (Sun et al. 2007; Kumar et al. 2008; Tripathi et al. 2009; Habibi et al. 2010; Mohammadalizadeh et al. 2011a, b; Keyvanloo et al. 2010; Farahzadi et al. 2012). In this work, the effects of three process variables (factors) of A: *zinc weight percent (%),* B: *temperature (°C)* and C: *space velocity* $(h^{-1})$ on the adsorption of $H_2S$ were investigated.

The parameters were normalized before analyzing the regression. The natural variables were coded as +1, −1 and 0 for high, low and central point, respectively. So the units of the parameters were not important. The actual variables $(X_i)$ were coded by linear transformation as follow:

$$x_i = \frac{X_i - \frac{(X_{\text{high}}+X_{\text{low}})}{2}}{\frac{(X_{\text{high}}+X_{\text{low}})}{2}} \tag{1}$$

where $x_i$ is the dimensionless coded value of $i$th factor, $X_i$ is the uncoded value of the $i$th independent variable (natural factor), and $X_{\text{high}}$ and $X_{\text{low}}$ are the uncoded factor value at high and low level, respectively. The three examined levels and experimental ranges of ZnO (denoted as A) are as follows: 5, 17.5 and 30 wt%. The three examined levels and experimental ranges of temperature (denoted as B) are as follows: 50, 175 and 300 °C. The three examined levels and experimental ranges of space velocity (denoted as C) are as follows: 3,000, 7,500 and 12,000 $h^{-1}$.

The behavior of the system was explained by the following quadratic polynomial equation as a function of independent variables involving their quadratic interactions and squared terms.

$$y = \beta_0 + \sum_{i=1}^{3} \beta_i x_i + \sum_{i=1}^{3} \beta_{ii} x_i^2 + \sum_{i=1}^{3} \sum_{i<j}^{3} \beta_i x_i x_j + \varepsilon \tag{2}$$

where $y$ is predicted response of the time at which the outlet concentration of $H_2S$ reaches 5,000 ppm, and $x_1$, $x_2$, $x_3$ are the coded independent variables, $\beta_0$ intercept, $\beta_i$ linear coefficient, $\beta_{ij}$ interaction quadratic coefficient, $\beta_{ii}$ squared coefficient, $i$ and $j$ are the index numbers for variables and $\varepsilon$ is the random error which shows the different sources of variability.

Least squares method was used to solve these set of equations (Keyvanloo et al. 2010; Farahzadi et al. 2012). The initial concentration of $H_2S$, 5,000 ppm, was taken as the criterion for $H_2S$ break point.

In statistics, Box–Behnken designs (BBD) are typical experimental design for response surface methodology. BBD is a class of rotatable or nearly rotatable second-order designs based on three-level incomplete factorial designs. Each design can be thought of as a combination of a two-level (full or fractional) factorial design with an incomplete block design. In each block, a certain number of factors are put through all combinations for the factorial design, while the other factors are kept at the central values.

The number of experiments ($N$) required for the development of BBD is defined as follows:

$$N = 2k(k-1) + C_o \tag{3}$$

where $k$ is number of factors and $C_o$ is the number of central points.

## Results and discussion

### XRD analysis

All prepared samples were characterized using low- and high-angle X-ray diffraction to get structural information

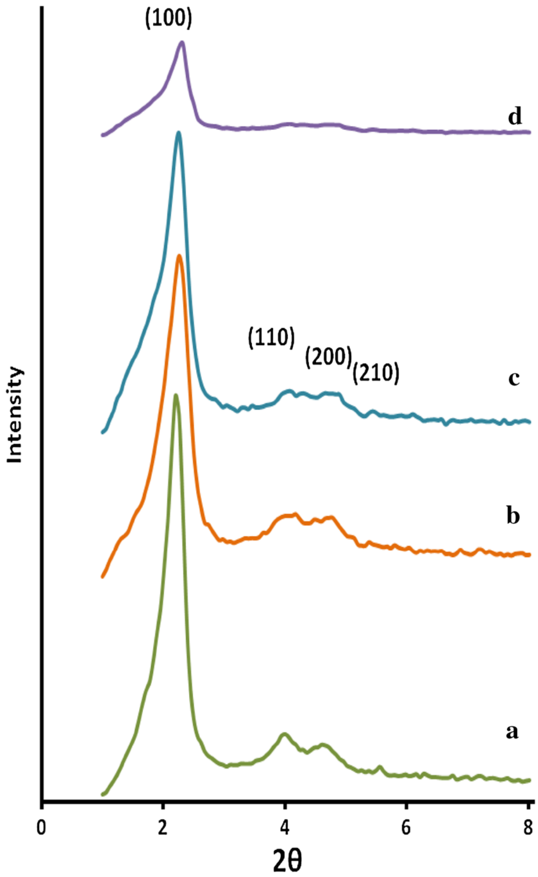

**Fig. 1** Low-angle X-ray diffraction patterns of **a** MCM-41, **b** ZnO5/MCM, **c** ZnO17.5/MCM and **d** ZnO30/MCM

about their pore order and phases of the obtained zinc oxide, respectively.

Low-angle X-ray diffraction patterns of zinc-containing MCM-41 samples are presented in Fig. 1a–d. The low-angle XRD patterns of all samples show an intense peak between 2.20 and 2.32° 2θ assigned to $d_{100}$ reflection which is characteristic of hexagonal mesoporous structure. As the amounts of zinc increases, the intensity of all reflections, especially $d_{100}$, decreases. This should be due to the collapsing of mesopores of MCM-41 as a result of formation of ZnO nanoparticles within the pores. Furthermore, the $d_{100}$ reflection shifted to lower 2θ angles after incorporation of zinc (Fig. 1b–d). The decrease in the *d-spacing* is caused by the lattice contraction originated from furtherer thermal treatment during incorporation of zinc. In the cases of MCM-41, ZnO5/MCM and ZnO17.5/MCM (Fig. 1a–c), the $d_{100}$ reflection was accompanied by weaker reflections at higher degree of $2\theta$ angles corresponding to the $d_{110}$, $d_{200}$ and $d_{210}$ reflections (hexagonal symmetry), respectively. These higher-order reflections indicate the presence of ordered hexagonal structure in the corresponding samples. But in the case of ZnO30/MCM, the $d_{100}$ reflection considerably weakened and $d_{110}$, $d_{200}$ and $d_{210}$ reflections were almost disappeared. This observation indicates that structural order in this sample distinctly decreased which is resulted by high metal loading. The high-angle XRD patterns of zinc incorporated samples show a peak on 36.5° 2θ assigned to $d_{101}$ reflection which indicates hexagonal zinc oxide crystals (Fig. 2).

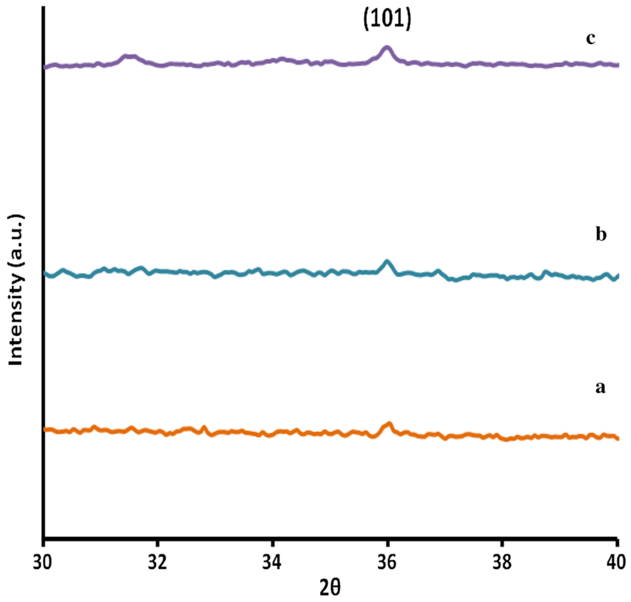

**Fig. 2** High-angle X-ray diffraction patterns of **a** ZnO5/MCM, **b** ZnO17.5/MCM **d** ZnO30/MCM

## Nitrogen physisorption

Nitrogen physisorption is a well-known technique for investigation of textural properties of porous materials. Adsorption isotherms of nitrogen for parent MCM-41, Zn5/MCM, ZnO17.5/MCM and ZnO30/MCM are shown in Fig. 3a–d, respectively. Parent MCM-41 (Fig. 3a) shows a type IV isotherm according to the IUPAC nomenclature which is a characteristic of mesoporous materials. The inflection of adsorption branch of isotherm at low relative pressure (0.2–0.3) is related to the filling of mesopores with liquid nitrogen via capillary condensation. The sharpness of this region of isotherm is an indication of structural order and size uniformity of mesopores. Desorption branch of isotherm almost coincides with the adsorption branch which is a furtherer suggestion of high uniformity of mesopores in this sample. Another feature of this region of isotherm is the absence of hysteresis loop implying that most of mesopores are directly connected to the surface of MCM-41 and are easily accessible for nitrogen molecules. The surface area (obtained from BET equation), pore volume and pore diameter of this sample, as well as the zinc-containing samples, were calculated and given in Table 1.

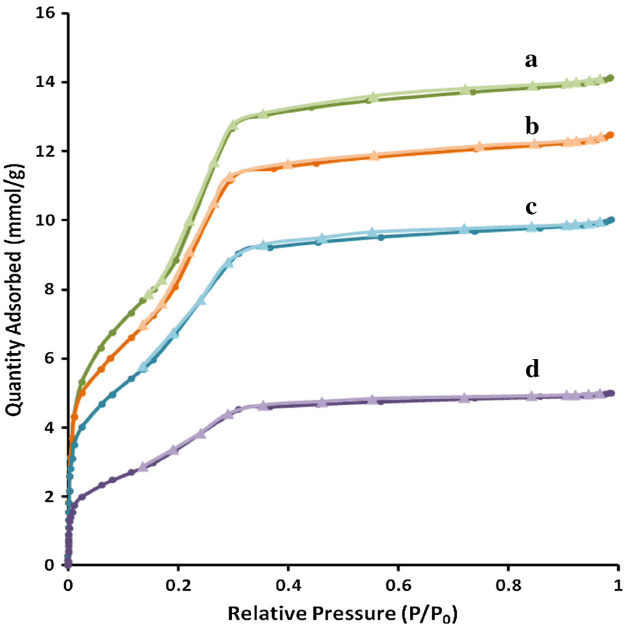

**Fig. 3** Nitrogen physisorption isotherm of **a** calcined MCM-41, **b** ZnO5/MCM, **c** ZnO17.5/MCM and **d** ZnO30/MCM

**Table 1** Textural properties of ZnO/MCM-41 samples containing different weight percent of zinc (0, 5, 17.5 and 30)

| Sample name | $S_{BET}$ (m$^2$/g) | $V_p$ (cm$^3$/g)[a] | $d$ (nm)[b] | a (nm)[c] | $W_d$ (nm)[d] | $b_d$ (nm)[e] |
|---|---|---|---|---|---|---|
| MCM-41 | 739 | 0.49 | 4.010 | 4.61 | 3.50 | 1.28 |
| ZnO5 | 680 | 0.43 | 3.908 | 4.49 | 3.32 | 1.33 |
| ZnO17.5 | 569 | 0.35 | 3.908 | 4.49 | 3.13 | 1.51 |
| ZnO30 | 254 | 0.14 | 3.802 | 4.37 | 2.24 | 2.24 |

[a] Mesopore volume

[b] d-spacing from XRD diffractograms

[c] Unit cell parameter

[d] Pore diameter (nm) calculated by geometrical method (Samadi-Maybodi et al. 2011)

[e] wall thickness obtained from $a - (w_d/1.050)$ equation

**Table 2** The design matrix and experimental data of the break point from the BBD design

| Run | Independent variables | | | |
|---|---|---|---|---|
| | A | B | C | $t_{bp}$ (min) |
| 1 | 17.5 | 175 | 7,500 | 180 |
| 2 | 30.0 | 175 | 12,000 | 119.4 |
| 3 | 17.5 | 50 | 3,000 | 355.3 |
| 4 | 30 | 50 | 7,500 | 446.1 |
| 5 | 5 | 50 | 7,500 | 157.6 |
| 6 | 17.5 | 175 | 7,500 | 179 |
| 7 | 17.5 | 175 | 7,500 | 170 |
| 8 | 5 | 300 | 7,500 | 216.4 |
| 9 | 17.5 | 175 | 7,500 | 192 |
| 10 | 30 | 175 | 3,000 | 634.4 |
| 11 | 5 | 175 | 12,000 | 283.1 |
| 12 | 5 | 175 | 3,000 | 241.1 |
| 13 | 17.5 | 50 | 12,000 | 172.1 |
| 14 | 30 | 300 | 7,500 | 459.3 |
| 15 | 17.5 | 175 | 7,500 | 185 |
| 16 | 17.5 | 300 | 3,000 | 850 |
| 17 | 17.5 | 300 | 12,000 | 190.2 |

The isotherm of ZnO5/MCM is shown in Fig. 3b. It demonstrates a type IV isotherm indicating that mesoporous structure of corresponding sample remained intact after incorporation of 5 wt% of zinc into MCM-41. The capillary condensation region almost coincides with capillary evaporation. This means that the uniformity of mesopores did not decrease after incorporation of zinc oxide into the mesopores of this sample. However, the height of capillary condensation/evaporation region slightly decreased and somewhat shifted to lower relative pressure. This observation results in small decrease in both mesopore volume and pore diameter which is caused by lattice contraction. Moreover, a parallel reason for decreasing of mesopore volume should be the occupation of mesopores with zinc oxide nanoparticles. In the case of ZnO17.5/MCM (Fig. 3c), the shape of isotherm corresponds to type IV and the capillary condensation/evaporation step is steel sharp. However, the decreasing of the height of this region of isotherm is able to be seen and is higher than that of ZnO5/MCM which is due to the higher amount of zinc oxide incorporated into MCM-41. Figure 3d shows the isotherm of ZnO30/MCM. As can be seen, the shape of isotherm obviously changed and the height of isotherm at capillary condensation/evaporation region considerably decreased. This should be due to the very high amount of zinc oxide incorporated into MCM-41 leading to the extreme collapse of mesopores. As the amounts of zinc increased, the mean pore diameter of the samples decreased. This should be due to the embedding of zinc oxide nanoparticles within the mesopores of the corresponding sample which leads to the decreasing of mean pore diameter. Another suggestion is the lattice contraction of zinc-containing samples caused by the subsequent thermal treatment during impregnation. This thermal treatment causes not only conversion of $Zn(NO_3)_2$ to ZnO nanoparticles but also a parallel reaction, i.e., condensation of silanol groups of MCM-41 to siloxane bond.

## Statistical analysis of $H_2S$ adsorption experiments

Based on Eq. 3, with 3 main factors and 5 times replication in center point to reduce the magnitude of error ($k = 3$ and $C_o = 5$), the runs will be limited to 17 as are detailed in

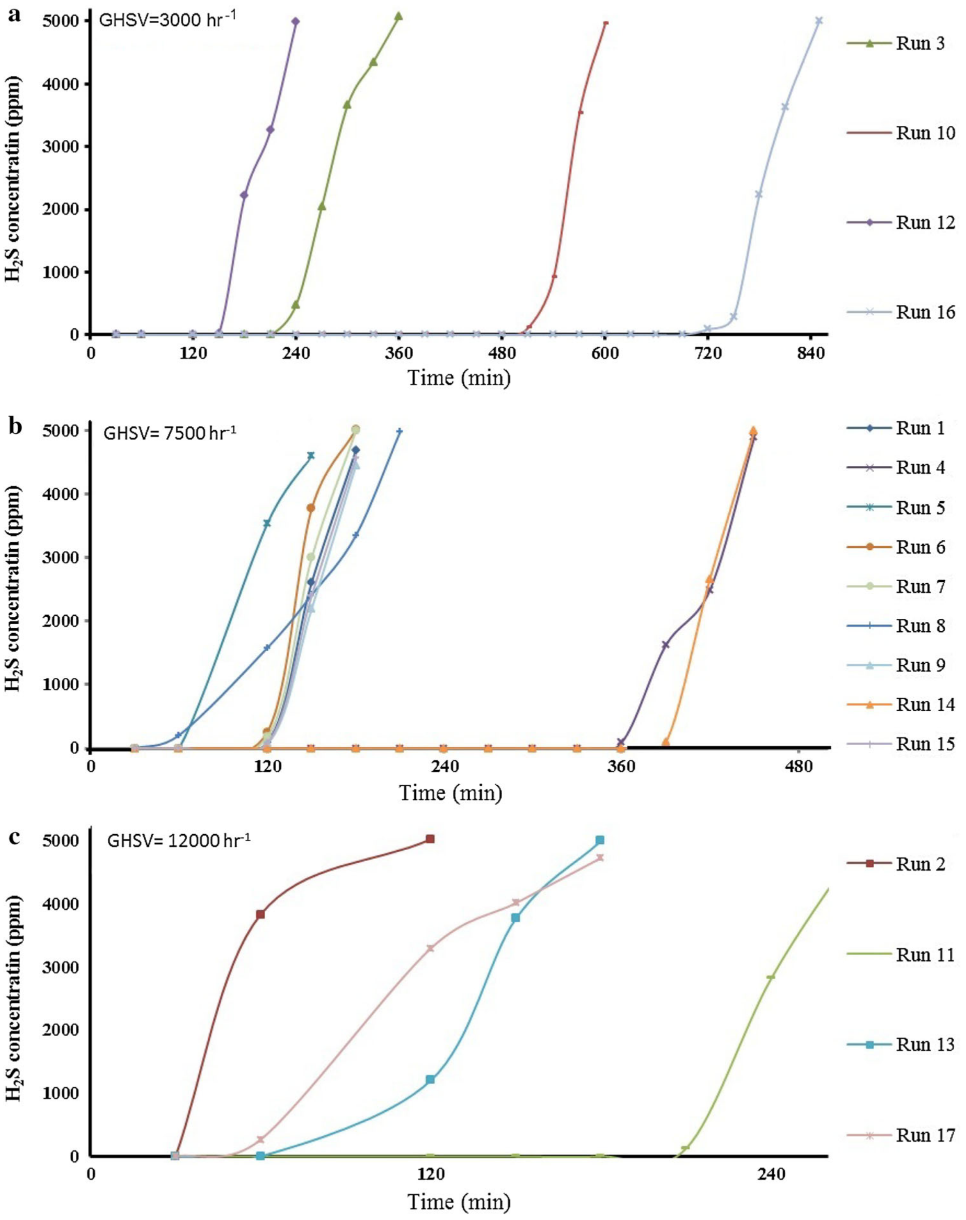

**Fig. 4** Breakthrough curves for adsorption of $H_2S$ on zinc-containing MCM-41. The *inset* at the *right side* of the figure represents the run number (Table 2)

Table 2. The obtained breakthrough curves for three space velocities, i.e., 3,000, 7,500 and 12,000 $h^{-1}$, were given in Fig. 4a–c, respectively. The breakthrough curves are shown in three figures because of large number of runs and also for easier understanding and interpretation of the obtained results. In this way, differences between $t_{bp}$ of runs can be understood more easily.

To decide about the adequacy of model for the $t_{bp}$, three different tests, sequential model sum of square, lack of fit test and model summary statistics were carried out in the present study.

The data of $t_{bp}$ in this research were subjected to regression analysis to estimate the effect of process variables.

The $p$ values for all the regressions were lower than 0.01 (Table 3). This means that at least one of the terms in the regression equation has a significant correlation with the response variables (Sun et al. 2007; Kumar et al. 2008). Model summary statistics showed that the excluding cubic model was aliased and quadratic model was found to have maximum "Adjusted R-Squared" and the "Predicted R-Squared" values. Therefore, quadratic model was chosen for further analysis.

The analysis of variance (ANOVA) calculation on $t_{bp}$ is summarized in Table 4. If the calculated value of $F$ is greater than that in the $F$ table at a specified probability level, a statistically significant factor or interaction is obtained (Mohammadalizadeh et al. 2011b; Keyvanloo

**Table 3** Adequacy of the model

| Source | Sum of square | *df* | Mean square | *F* value | Prob > *F* | Remark |
|---|---|---|---|---|---|---|
| *Sequential model sum of square* | | | | | | |
| Mean | $1.489 \times 10^6$ | 1 | $1.489 \times 10^6$ | | | |
| Linear | $3.316 \times 10^5$ | 3 | $1.105 \times 10^5$ | 4.87 | 0.0175 | Suggested |
| 2FI | $1.349 \times 10^5$ | 3 | 44,956.33 | 2.81 | 0.0943 | Suggested |
| Quadratic | $1.072 \times 10^5$ | 3 | 35,722.22 | 4.71 | 0.0419 | Suggested |
| Cubic | 52,785.95 | 3 | 17,595.33 | 267.81 | <0.0001 | Aliased |
| Residual | 262.80 | 4 | 65.70 | | | |
| Total | $2.116 \times 10^6$ | 17 | $1.244 \times 10^5$ | | | |
| *Lack of fit tests* | | | | | | |
| Linear | $2.948 \times 10^5$ | 9 | 32,757.96 | 498.6 | <0.0001 | Suggested |
| 2FI | $1.600 \times 10^5$ | 6 | 26,658.78 | 405.77 | <0.0001 | Suggested |
| Quadratic | 52,785.98 | 3 | 17,595.33 | 267.81 | <0.0001 | Suggested |
| Cubic | 0.000 | 0 | | | | Aliased |
| Pure error | 0.029 | 4 | 65.70 | | | |

| Source | SD | $R^2$ | Adjusted $R^2$ | Predicted $R^2$ | PRESS | Remark |
|---|---|---|---|---|---|---|
| *Model summary statistics* | | | | | | |
| Linear | 150.66 | 0.5291 | 0.4205 | 0.1161 | $5.540 \times 10^5$ | Suggested |
| 2FI | 126.58 | 0.7444 | 0.5910 | 0.1093 | $5.582 \times 10^5$ | Suggested |
| Quadratic | 87.05 | 0.9154 | 0.8065 | −0.3483 | $8.450 \times 10^5$ | Suggested |
| Cubic | 8.11 | 0.9996 | 0.9983 | | | Aliased |

**Table 4** Analysis of variance (ANOVA) of the response surface model for the prediction of $t_{\mathrm{bp}}$

| Source | Sum of square | *df* | Mean square | *F* value | *P* value (Prob > *F*) | Remark |
|---|---|---|---|---|---|---|
| Model | $5.737 \times 10^5$ | 9 | 63,739.63 | 8.41 | 0.0052 | Significant |
| A | 72,390.13 | 1 | 72,390.13 | 9.55 | 0.0176 | Significant |
| B | 42,748.88 | 1 | 42,748.88 | 5.64 | 0.0492 | Significant |
| C | $2.165 \times 10^5$ | 1 | $2.165 \times 10^5$ | 28.57 | 0.0011 | Significant |
| AB | 519.84 | 1 | 519.84 | 0.069 | 0.8009 | Not significant |
| AC | 77,562.25 | 1 | 77,562.25 | 10.23 | 0.0151 | Significant |
| BC | 56,786.89 | 1 | 56,786.89 | 7.49 | 0.0290 | Significant |
| $A^2$ | 4,620.07 | 1 | 4,620.07 | 0.61 | 0.4605 | Not significant |
| $B^2$ | 46,886.42 | 1 | 46,886.42 | 6.19 | 0.0418 | Significant |
| $C^2$ | 46,575.92 | 1 | 46,575.92 | 6.15 | 0.0423 | Significant |
| Error | 262.80 | 4 | 65.70 | | | |
| Total | $6.267 \times 10^5$ | 16 | | | | |

et al. 2010). The $F$ is defined as $F = \mathrm{MSF/MSE}$, where MSF and MSE are the mean squares of factors (interactions) and mean squares of errors, respectively. After carrying out the ANOVA test, the factors $A$, $B$, $C$ and interactions $A \times C$, $B \times C$, $B^2$ and $C^2$ proved to have statistically significant effect on $t_{\mathrm{bp}}$, but interactions $A \times B$ and $A^2$ exhibited statistically insignificant effect on $t_{\mathrm{bp}}$. $F$ value is an indication of the level of significance. The higher $F$ is the more significant effect on the response. From a combination of estimates for the variables and the ANOVA results, a quadratic model with statistical significance can be generated. The regression equation obtained after variance analysis gives the level of $H_2S$ adsorption. It includes a linear relationship between all the main effects and response the final quadratic polynomial equations in terms of natural variables presented as follows:

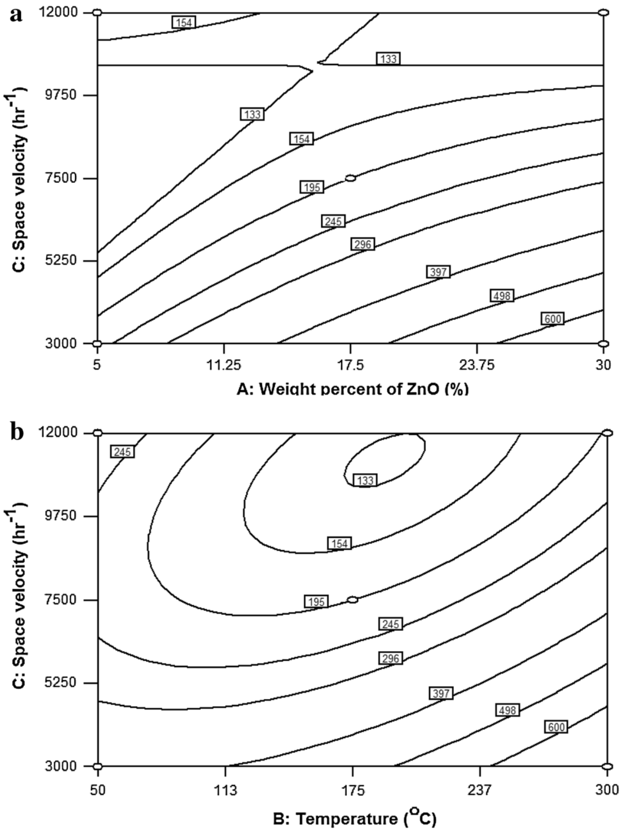

**Fig. 5** Contour plots describing the response surface $t_{bp}$ in min as a function of **a** Weight percent of zinc versus space velocity (Temperature: 175° C), **b** temperature versus space velocity (zinc loading: 17.5 wt%)

$$\begin{aligned} t_{bp} = &+158.481 + 20.033X_A - 0.063X_B - 0.0341X_C \\ &- 7.296 \times 10^{-3}X_A \cdot X_B - 2.476 \times 10^{-3}X_A \cdot X_c \\ &- 2.118 \times 10^{-4}X_B \cdot X_C + 0.212X_A^2 + 6.754 \times 10^{-3}X_B^2 \\ &+ 5.194 \times 10^{-6}X_C^2 \end{aligned} \tag{4}$$

However, in this equation, the insignificant terms, i.e., $A^2$ and *AB,* were omitted, and the equation was refitted to experimental data. The obtained Eq. (5) is as follows:

$$\begin{aligned} t_{bp} = &+138.107 + 26.177X_A - 0.229X_B - 0.0354X_C \\ &- 2.476 \times 10^{-3}X_A \cdot X_c - 2.118 \times 10^{-4}X_B \cdot X_C \\ &+ 6.865 \times 10^{-3}X_B^2 + 5.279 \times 10^{-6}X_C^2 \end{aligned} \tag{5}$$

$X_i$ denotes the actual variables for factors, i.e., *A*, *B* and *C*. $X_A$ corresponds to the weight percent of zinc (wt%) in the adsorbent, $X_B$ (°C) to the temperature and $X_C$ ($h^{-1}$) to the space velocity. The $R^2$ value equals to 0.9072 for Eq. (5) indicates a good fitting for the experimental data of the break point time.

## Effects of the model components and their interactions on $t_{bp}$

According to this figure, break point increases by increasing the weight percent of zinc (A) in the adsorbents and decreased by increasing the space velocity (C). Increasing zinc loading at center point operating condition (T: 175 °C and space velocity: 7,500 $h^{-1}$) caused noticeable increasing of $t_{bp}$. This is attributed to rise in the active sites by increasing zinc oxide loading on MCM-41 which increases the chemisorption of $H_2S$ on the support materials by increasing temperature, $t_{bp}$ also increases. Increasing the temperature speeded up the adsorption of $H_2S$ by chemical adsorption of $H_2S$ on ZnO (Maghsodi et al. 2013). However, we performed TGA test on three spent adsorbents which adsorbed $H_2S$ at 50, 140 and 300 °C, respectively). The first adsorbent showed a reduction peak of about 3 % at 150 °C, the second adsorbent displayed a reduction weight about 1.9 % at 150 °C and the third adsorbent exhibited 5.9 % weight loss at 530 °C. This means that weight reduction at 150 °C temperature is due to the release of physically adsorbed $H_2S$ on adsorbent. The weight reduction at higher temperature (5.9 %) is larger than those of low temperatures (3 and 1.9 %). This larger weight loss at high temperature indicates that type of adsorption at high temperature is chemisorption.

## Contour plots

Contour plots can be used to study the effects of process variables on the adsorption of $H_2S$ in a wider range of operating conditions. Furthermore, it can also be used for designing optimum conditions for the adsorption of $H_2S$. Eq. (5) was used to construct the contour plots for $t_{bp}$ against the zinc weight percent, temperature and space velocity as shown in Fig. 5. At constant weight percent of zinc, $t_{bp}$ decreases with increasing of space velocity and then increases (Fig. 5a). The steepness of decreasing of $t_{bp}$ is high at low ZnO wt%, but it is considerably low at high ZnO wt%. The break point is maximized at high level of ZnO wt% and low level of space velocity. From Fig. 5b, the break point time is maximized at high level of temperature and low level of space velocity. The optimum condition, i.e., Zn = 30 wt%, $T = 300$ °C and space velocity = 3,000 $h^{-1}$, gives the highest break point time equal to 973 min. According to the Table 3 (ANOVA Table), $A^2$ and *AB* were insignificant terms in Eq. (4) and so they were omitted and then this equation was refitted to experimental data to yield Eq. (5). After refitting of the model, contour plot which represents the interaction of *A* (ZnO wt%) and *B* (temperature) was removed, but interaction of AC and BC was illustrated in Fig. 5a, b, respectively.

## Conclusion

In this work, the $H_2S$ content of crude oil was removed using combination of two methods, i.e., stripping and adsorption. Investigation in to effects process parameters including weight percent of zinc, temperature of adsorption and space velocity on the adsorption of $H_2S$ using ZnO*x*/MCM was also carried out via RSM methodology and Box–Behnken experimental design. Characterization tests (XRD and $N_2$ physisorption) showed that up to 30 wt% of ZnO, ordered hexagonal structure of MCM-41 preserved. After carrying out the ANOVA test, the factors *A*, *B*, *C* and interactions $A \times C$, $B \times C$, $B^2$ and $C^2$ proved to have statistically significant effect on $t_{bp}$, but interactions $A \times B$ and $A^2$ exhibited statistically insignificant effect on $t_{bp}$. Among the main effects, space velocity has the highest effect on the response, while temperature has the lowest effect. Among interactions, $A \times C$ has the highest effect on the response even higher than those of two main effects, i.e., temperature and ZnO wt%. The regression equation obtained after variance analysis gives the level of $H_2S$ adsorption. According to *F* value, the obtained model is significant and $R^2$ is larger than 0.90 providing that over 90 % of total variations is explained by the model. Furthermore, according to *F* value, the *lack of fit* is not significant relative to the pure error which means the model capture all the assignable cause variation of the response. The optimal values of key factors (zinc loading, temperature and space velocity) were obtained by solving the regression Eq. 4. The point of weight percent of Zn $= 30$ wt%, $T = 300$ °C and space velocity $= 3{,}000\ \mathrm{h}^{-1}$ in experimental design is the optimum point with the highest break point. The adsorption of $H_2S$ from crude oil has a high impact on oil industry and environment because it reduces the emission of $H_2S$ and saves the loss of valuable LPG and lighter gases.

**Acknowledgments** We would like to acknowledge the Iranian national oil company for the financial support under the grant number of 14832662. This work has been supported by Iranian national oil company. This work is original and is not published previously and also is not under consideration elsewhere. All authors are agreeing with publication of this manuscript in *International Journal of Environmental Science and Technology*.

## References

Bagreev A, Menendez JA, Dukhno I, Tarasenko Y, Bandosz TJ (2004) Bituminous coal-based activated carbons modified with nitrogen as adsorbents of hydrogen sulfide. Carbon 42(3):469–476

Corma A, Martinez A, Martinezsoria V, Monton JB (1995) Hydrocracking of vacuum gasoil on the novel mesoporous MCM-41 aluminosilicate catalyst. J Catal 153(1):25–31

Dorman DC, Moulin FJ, McManus BE, Mahle KC, James RA, Struve MF (2002) Cytochrome oxidase inhibition induced by acute hydrogen sulfide inhalation: correlation with tissue sulfide concentrations in the rat brain, liver, lung, and nasal epithelium. Toxicol Sci 65(1):18–25

Farahzadi M, Towfighi J, Mohammaalizadeh A (2012) Catalytic oxidation of isopropyl mercaptan over nano catalyst of tungsten oxide supported multiwall carbon nanotubes. Fuel Process Technol 97:15–23

Galarneau A, Desplantier D, Dutartre R, Direnzo F (1999) Micelle templated silicates as a test bed for methods of mesopore size evaluation. Microp. Mesop. Mater. 27(2–3):297–308

Habibi R, Rashidi AM, Towfighi-Daryan J, Mohammadalizadeh A (2010) Study of the Rod-Like and spherical nano-ZnO morphology on H2S removal from natural gas. Appl Surf Sci 257(2):434–439

Hogan CM (2010) Abiotic factor encyclopedia of earth. In: Monosson E, Cleveland C (eds).National Council for Science and the Environment, Washington DC

Holleman AF, Wiberg E (2001) Inorganic chemistry. Academic Press, San Diego

Husein MM, Patruyo L, Pereira-Almao P, Nassar NN (2010) Scavenging H2S(g) sorption from oil phases by means of ultradispersed sorbents. J Colloid Interface Sci 342(2):253–260

Keyvanloo K, Towfighi J, Sadrameli SM, Mohamadalizadeh A (2010) Investigating the effect of key factors, their interactions and optimization of naphtha steam cracking by statistical design of experiments. J Anal Appl Pyrolysis 87(2):224–230

Ko TH, Chu H, Chaung LK, Tseng TK (2004) High temperature removal of hydrogen sulfide using an N-150 sorbent. J Hazard Mater 114(1–3):145–152

Kresge CT, Leonowicz ME, Roth WJ, Vartuli JC, Beck JS (1992) Ordered mesoporous molecular sieves synthesized by a liquid-crystal template mechanism. Nature 359:710–712

Kumar A, Prasad B, Mishra I (2008) Optimization of process parameters for acrylonitrile removal by a low-cost adsorbent using Box–Behnken design. J Hazard Mater 150(1):174–182

Li L, Wu P, Yu Q, Wu G, Guan N (2010) Low temperature $H_2$-SCR over platinum catalysts supported on Ti-containing MCM-41. Appl Catal B Environ 94(3–4):254–262

Maghsodi H, Soltanieh M, Bozorgzadeh HR, Mohamadalizadeh A (2013) Adsorption isotherms and ideal selectivities of hydrogen sulfide and carbon dioxide over methane for the Si-CHA zeolite: comparison of carbon dioxide and methane adsorption with the all-silica DD3R zeolite. Adsorption 19:1045–1053

Mohammadalizadeh A, Towfighi J, Rashidi A, Manteghian M, Mohajeri A, Arasteh R (2011a) Nanoclays as nano adsorbent for oxidation of $H_2S$ into elemental sulfur. Korean J Chem Eng 28(5):1221–1226

Mohammadalizadeh A, Towfighi J, Rashidi A, Mohajeri A, Golkar M (2011b) Modification of carbon nanotubes for $H_2S$ sorption. Ind Eng Chem Res 50(13):8050–8057

Morais Batista AH, de Sousa FF, Honorato SB, Ayala AP, Filho JM, de Sousa FW, Pinheiro AN, de Araujo JCS, Nascimento RF, Valentini A, Oliveira AC (2010) Ethylbenzene to chemicals: catalytic conversion of ethylbenzene into styrene over metal-containing MCM-41. J Mol Catal A: Chem 315(1):86–98

Nassar NN, Husein MM, Pereira-Almao P (2010) Ultradispersed particles in heavy oil: part II, sorption of $H_2S$ (g). Fuel Process Technol 91(2):169–174

Polychronopoulou K, Fierro JLG, Efstathiou AM (2005) Novel Zn–Ti-based mixed metal oxides for low-temperature adsorption of $H_2S$ from industrial gas streams. Appl Catal B Environ 57(2):125–137

Rowan FE, Docherty NG, Coffey JC, O'Connell PR (2009) Sulphate-reducing bacteria and hydrogen sulphide in the aetiology of ulcerative colitis. Br J Surg 96(2):151–158

Samadi-Maybodi A, Teymouri M, Vahid A, Miranbeigi A (2011) In situ incorporation of nickel nanoparticles into the mesopores of MCM-41 by manipulation of solvent-solute interaction and its activity toward adsorptive desulfurization of gas oil. J Hazard Mater 192(3):1667–1674

Srivastav A, Srivastava VC (2009) Adsorptive desulfurization by activated alumina. J Hazard Mater 170(2–3):1133–1140

Subrenat A, Le Leuch LM, Le Cloirec P (2008) Electro deposition of copper and iron oxides on to activated carbon fibred cloths: application to $H_2S$ and $NH_3$ removal from air. Environ Technol 29(9):993–1000

Sun J, Modi S, Liu K, Lesieur R, Buglass J (2007) Kinetics of zinc oxide sulfidation for packed-bed desulfurizer modeling. Energ Fuels 21(4):1863–1871

Taguchi A, Schuth F (2005) Ordered mesoporous materials in catalysis. Microp Mesop Mater 77(1):1–45

Tripathi P, Srivastava V, Kumar A (2009) Optimization of an azo dye batch adsorption parameters using Box–Behnken design. Desalin. 149(3):1273–1279

Untea I, Dancila M, Vasile E, Belcu M (2009) Structural, morphological and textural modifications of ZnO–$TiO_2$ HTGD based sorbents induced by $Al_2O_3$ addition, thermal treatment and sulfurizing process. Powder Technol 191(1–2):27–33

Wan Y, Zhao DY (2007) On the controllable soft-templating approach to mesoporous silicates. Chem Rev 107(7):2821–2860

Wang X, Jia J, Zhao L, Sun T (2008) Chemisorption of hydrogen sulphide on zinc oxide modified aluminum-substituted SBA-15. Appl Surf Sci 254(17):5445–5451

Wang JA, Zhou XL, Chen LF, Norena LE, Yu GX, Li CL (2009) Hydroisomerization of n-heptane on the Pt/$H_3PW_{12}O_{40}$/Zr-MCM-41 catalysts. J Mol Catalysis A Chem 299(1–2):68–76

Wang J, Qiu B, Han L, Feng G, Hu Y, Chang L, Bao W (2012) Effect of precursor and preparation method on manganese based activated carbon sorbents for removing $H_2S$ from hot coal gas. J Hazard Mater 213–214:184–192

Westmoreland PR, Harrison DP (1976) Evaluation of candidate solids for high-temperature desulfurization of low-Btu gases. Environ Sci Technol 10(7):659–661

Wieckowska J (1995) Catalytic and adsorptive desulphurization of gases. Catal Today 24(4):405–465